Magnetic Resonance Letters 1 (2021) 11–27

Contents lists available at ScienceDirect

Magnetic Resonance Letters

journal homepage: www.keaipublishing.com/MRL

Review Article

Progresses of hyperpolarized ^{129}Xe NMR application in porous materials and catalysis

Benhan Fan [a, c], Shutao Xu [a, *], Yingxu Wei [a, *], Zhongmin Liu [a, b, *]

[a] National Engineering Laboratory for Methanol to Olefins, Dalian National Laboratory for Clean Energy, iChEM (Collaborative Innovation Center of Chemistry for Energy Materials), Dalian Institute of Chemical Physics, Chinese Academy of Sciences, Dalian, 116023, China
[b] State Key Laboratory of Fine Chemicals, School of Chemical Engineering, Dalian University of Technology, Dalian, 116024, China
[c] University of Chinese Academy of Sciences, Beijing, 100049, China

ARTICLE INFO

Article history:
Received 1 December 2020
Received in revised form 5 February 2021
Accepted 13 February 2021
Available online 15 June 2021

Keywords:
Solid-state NMR
Hyperpolarized ^{129}Xe
Review
Porous materials
Catalysis

ABSTRACT

^{129}Xe NMR has been proven to be a powerful tool to investigate the structure of porous materials. Xenon is a monatomic noble gas which could be used as a probe due to the extremely sensitive to its local environment. Optical pumping techniques for production of hyperpolarized (HP) xenon have led to an increase of sensitivity up to orders of magnitude compared with traditional ^{129}Xe NMR. This review summarizes the application of this technique in porous materials and heterogeneous catalysis in recent ten years, involving of zeolites, metal-organic frameworks (MOFs), catalytic process and kinetics.

1. Introduction

Xenon, an inert monatomic gas with a van der Waals diameter of 0.44 nm, is colorless, odorless, and non-flammable which does not react easily with other substances. It has nine stable isotopes whereas only ^{129}Xe ($I = 1/2$) and ^{131}Xe ($I = 3/2$) can be used in NMR technology attribute to their nonzero spin [1]. ^{131}Xe with a natural abundance of 26.2% has attracted much less attention due to the electric quadrupole moment. On the opposite, ^{129}Xe is much more frequently used in NMR spectroscopy both in terms of its natural abundance of 26.4% (Its sensitivity is approximately 5.60×10^{-3} and 31.8 with respect to ^{1}H and ^{13}C, respectively), and particularly its enormous chemical shift range from δ −40 to δ 7500 [2].

In the early 1980s, Ito [3] and Ripmeester [4] first brought xenon into NMR to study porous solids just because xenon gas is not only with less reactive but also sensitive to the changes of its surrounding environment. Under the research background at that time, Xe NMR emerged at a proper time and developed rapidly in the following 30 years. With the unique properties and many potential applications, ^{129}Xe NMR is a powerful technology which has been widely used in many fields, such as zeolites [5–7], metal-organic frameworks (MOFs) [8–12] and organic polymers [13].

Xenon has the very large electron cloud which is extremely polarizable. When it is adsorbed in porous materials, any little changes taken place in structures or confined environment will influence the chemical shift. There are many factors could be influence the chemical shift of xenon atom which is expressed by the following formula [3]:

* Corresponding authors:
E-mail addresses: xushutao@dicp.ac.cn (S. Xu), weiyx@dicp.ac.cn (Y. Wei), liuzm@dicp.ac.cn (Z. Liu).
Peer review under responsibility of Innovation Academy for Precision Measurement Science and Technology (APM), CAS.

https://doi.org/10.1016/j.mrl.2021.100005

$$\delta = \delta_0 + \delta_S + \delta_{Xe-Xe} + \delta_{SAS} + \delta_E + \delta_M \quad (1)$$

δ_0 is usually used as a reference which represents the xenon in gaseous phase at zero pressure, δ_S is in connection with the pore structure which represents the interaction of xenon atom on the surface of materials. $\delta_{Xe\text{-}Xe}$ is related to the concentration of xenon gas which expresses the collisions of xenon atoms inside the pore, thus, $\delta_{Xe\text{-}Xe}$ can be ignored when the density of xenon is reduced to a certain extent. Different metal particles or highly charged cations are identified as the strong adsorption sites inside the pore will influence the δ_{SAS}. δ_E and δ_M are the contributions of the electric and magnetic field of the cations. δ_E and δ_M can be ignored for small ions such as Na^+, Li^+, and H^+ for cation exchanged zeolites.

The chemical shifts detected by ^{129}Xe NMR are affected by various chemical environments in which Xe nuclei are located, however, the relaxation time of xenon nuclei in amorphous materials and mesoporous zeolites is relative longer. This factor had limited the further development of ^{129}Xe NMR technology. At the same time, improving the sensitivity of ^{129}Xe NMR is another challengeable requirement work. With the development of new technologies, the detection sensitivity could be improved by 10^4 times and relaxation time can be greatly reduced by using hyperpolarized (HP) ^{129}Xe.

The nuclear spin polarization of conventional ^{129}Xe NMR is governed by Boltzmann equilibrium. Using spin-exchange and optical-pumping techniques (SEOP) to generate HP ^{129}Xe which can break Boltzmann equilibrium and raise sensitivity to a rather high range [14]. That is why more and more HP ^{129}Xe are widely used not only in NMR fields but also extend to nuclear magnetic resonance imaging (MRI) [15–19].

2. Basic principle and technique of HP ^{129}Xe NMR

In the early 1950s, Kastler [20] first discovered the balance of nuclear spin energy level could be changed by polarized light. Almost 10 years later, Bouchiat [21] found the phenomenon that optical polarization of alkali metal such as rubidium can be transferred to rare gas through Overhauser effect. The first polarized ^{129}Xe NMR spectrum was observed by Happer [22] in the 1980s. In 1991, optical pumping technology was successfully used in physical adsorption of Xe NMR by Pines [23]. Zeng [24] obtained the signal of ^{129}Xe NMR by the spin-exchange cesium. The fundamental principle of SEOP techniques were explained in detail below.

2.1. Optical pumping

Highly nuclear spin polarization can be obtained by using optical pumping to break the nuclear spin distribution in thermal equilibrium (see Fig. 1) [14]. Optical pumping method, which was first shown by Kastler, achieves highly non-Boltzmann population distribution by exploiting the quantum mechanical selection rules of angular momentum [20]. Alkali-metal atoms can be optically pumped at the wavelength of their D_1 transition (975 nm for Rb). The electronic energy levels of the alkali-metal atoms split into $(2J + 1)$ sub-levels in the presence of the external magnetic field. J is the quantum

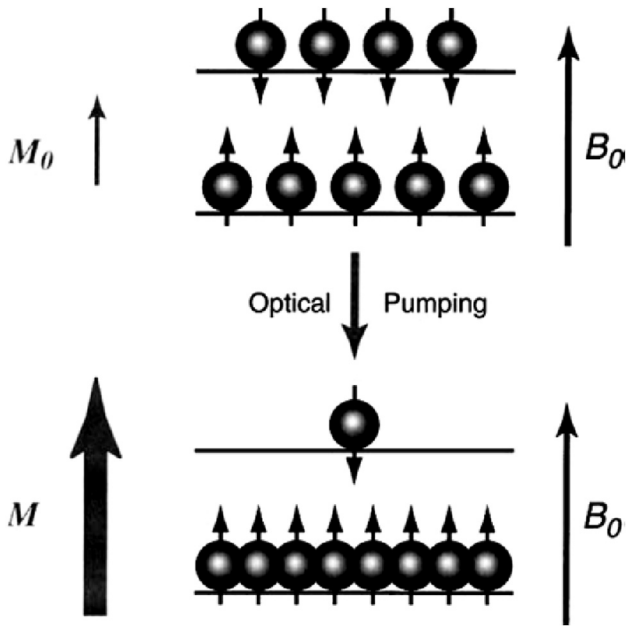

Fig. 1. Cartoon depicting the effect of laser-polarization for a collection of spin 1/2 nuclei. Adapted with permission [14]. Copyright 2002, Elsevier.

number of the electronic angular momentum. Electronic energy levels $S_{1/2}$ and $P_{1/2}$ are involved in the D_1 transition of alkali-mental atoms. Irradiation of circularly polarized δ^+ light results in an electronic transition from the ground state ($S_{1/2}$) sublevel with $m_J = -1/2$ to the excited state ($P_{1/2}$) sublevel with $m_J = +1/2$. The optically pumped alkali-metal atoms return within about 30 ns into the two ground-state ($S_{1/2}$) sublevels with $m_J = \pm 1/2$. During the transition, fluorescence will be emitted. The alkali metal atoms will lose polarization if the fluorescence is re-absorbed. Therefore, a buffer gas (common N_2) is added to quench the fluorescence. For the whole process, the number of $m_J = +1/2$ in the ground state is increasing, on the opposite, the number of electrons in $m_J = -1/2$ is decreasing due to continuous optical pumping (see Fig. 2(a)).

2.2. Spin exchange

Spin exchange refers to the process of transferring the spin angular momentum of electrons from alkali-metals to nuclei of inert gases (see Fig. 2(b)). Optically pumped alkali-metal atoms can exchange their electron spin polarization with other spins. The spin-exchange between optically pumped alkali-metal atom and ^{3}He occurs predominantly during binary collisions. The spin-exchange between optically pumped alkali-metal atoms and heavier noble gases such as ^{129}Xe is mediated by the formation of van der Waals molecules, especially at relatively low pressures. The nuclear polarization P of the noble gas after a given duration of optical pumping (t) is governed by the relation [25,26]:

$$P = \frac{\rho_{SE}}{\rho_{SE} + \rho_0} P_{Rb}\left[1 - e^{-(\rho_{SE}+\rho_0)t}\right] \tag{2}$$

Where P_{Rb} is the electron spin polarization of the Rb, ρ_{SE} is the rate of spin exchange between the noble gas nuclei and the rubidium electrons, and ρ_0 contains all other contributions to the longitudinal relaxation of the noble gas nuclei. As a consequence, the optical pumping and spin exchange can obtain a higher spin polarization of non-equilibrium nuclei and increase the polarizability by 4–5 orders of magnitude [14,25].

2.3. Continuous flow and magic angle spinning technology

In situ continuous flow (CF) and magic angle spinning (MAS) techniques also developed in HP ^{129}Xe NMR. MAS technology which spinning the NMR rotor at the magic angle θ_m (54.74°, where $1-3\cos^2\theta_m = 0$), can increase the resolution through eliminated the anisotropy of solid samples which can easily identify and analyze the NMR spectrum [27,28].

In situ NMR studies of heterogeneous catalytic, the reaction condition such as temperature, pressure and gas flow rate of reaction are best closely to the real chemical reactions and cooperated with chromatography (GC) and mass spectrometry (MS) to evaluate the reactivity of catalytic reactions [29]. The reaction was conducted under the CF condition for the majority of industrial catalytic processes, so it also drives the workers committed to the development for *in situ* solid-state NMR flow reactor. In order to solve this problem, the first step is to obtain a narrow spectral line by sampling the rotor under MAS condition. Secondly, the integrity of samples should be maintained in the process of flowing atmosphere passing through the

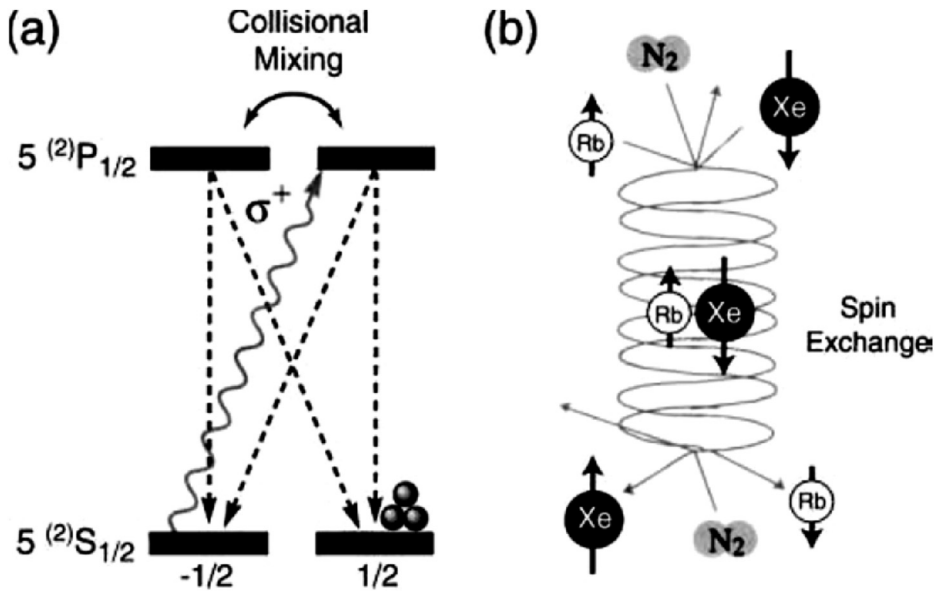

Fig. 2. Cartoons of the alkali-metal optical-pumping (a) and spin-exchange processes (b). Adapted with permission [14]. Copyright 2002, Elsevier.

rotor. Despite there are many technical difficulties, some international laboratories still focused on this field and achieved excellent results [30–34]. In 1995, Hunger [30] first use the NMR rotor as a fix-bed reactor to imitate real catalytic reaction at the condition of MAS and CF of reactants. The first CF MAS probe was improved by Hunger with a commercial Bruker 7 mm MAS probe [35]. Hunger et al. used this CF MAS probe to study the mechanism of methanol-to-olefin (MTO) process and proposed that the surface methoxy species play an important role in the formation of "hydrocarbon pool" [36–38]. Xu et al. [39] studied the reaction kinetics in nano-confined space using *in situ* HP ^{129}Xe NMR together with CF and MAS methods (Fig. 3).

3. HP ^{129}Xe NMR applied in porous materials

According to different pore sizes, porous materials can be classified into microporous ($d < 2$ nm), mesoporous ($2\ \text{nm} \leq d < 50$ nm) and macroporous ($d \geq 50$ nm) [40]. Microporous materials have unique crystal and channel structures, which not only determine their special shape selectivity catalysis, but also exhibit the strong adsorption and separation performance. On the other hand, the small pore size has also limited the diffusion in the process of macromolecular catalytic reactions. Mesoporous materials have large pore size, uniform pore structure and flexible composition, which can be used as catalysts and carries for macromolecular catalytic reactions. For macromolecular reactions or viscous system with minimal diffusion, macroporous materials can improve catalytic performance more effectively. ^{129}Xe NMR is one of the most effective and sensitive methods to detect porous materials, make good use of HP technology could greatly improve detection sensitivity and reduce testing time, especially in the situation of a small number of samples, low specific surface area, and nonequilibrium process. This section mainly introduced the applications of HP ^{129}Xe NMR in zeolites and MOFs [41–43].

3.1. Zeolites

As an important member of inorganic porous material, zeolites have a regular pore channel structure, a large specific surface area and a molecular size of a channel which can be widely used in the fields of catalysis, ion exchange, gas adsorption, and separation [44].

In 1982, Fraissard and Ripmeester first introduce ^{129}Xe probe into the catalytic system of zeolites, and since then, ^{129}Xe NMR technology developed rapidly from conventional ^{129}Xe to HP ^{129}Xe NMR with the additional CF and MAS techniques. One-dimensional corresponding with two-dimensional HP ^{129}Xe NMR spectrums can clearly study pore structure and connectivity, distribution of guest particles, location of coke deposition, and diffusion process of adsorbed molecules on the surface [45].

3.1.1. Pore structure and connectivity

In general, properties of a single zeolite cannot accommodate all the requirements, so the combination of two or more zeolites with different pore structures or different properties by means of synthesis may represent a good synergistic effect

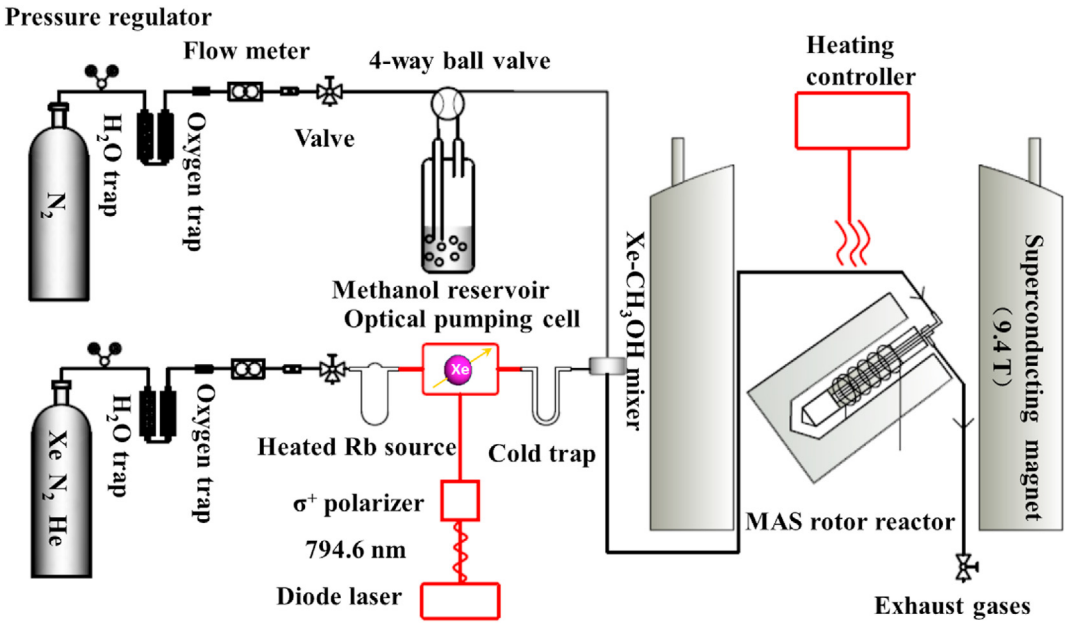

Fig. 3. Schematic representation of *in situ* CF HP ^{129}Xe MAS NMR. Adapted with permission [39]. Copyright 2008, American Chemical Society.

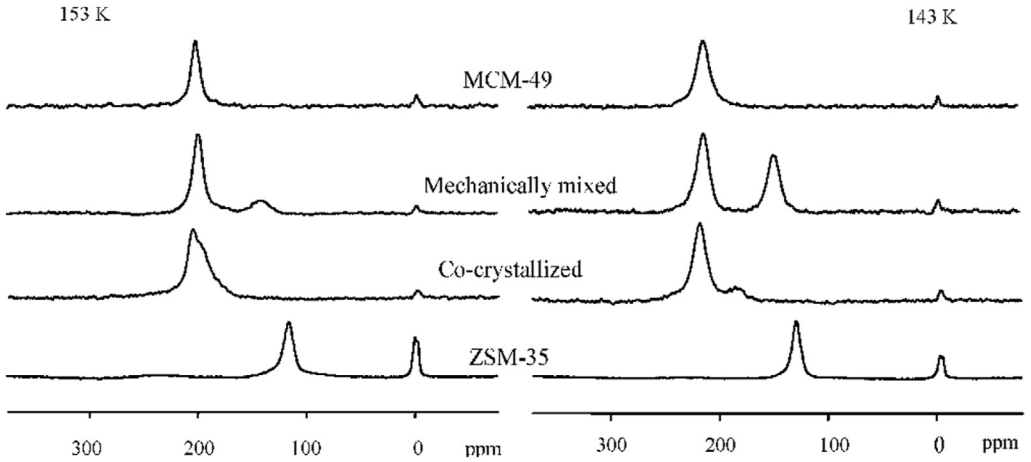

Fig. 4. HP ^{129}Xe NMR spectra of Xe adsorbed in MCM-49, mechanically mixed, co-crystallized, and ZSM-35 zeolites at 153 K and 143 K. Adapted with permission [46]. Copyright 2008, American Chemical Society.

that a single zeolite does not have. The co-crystallized and hierarchical pores zeolites are the most discussed composite porous molecular sieves in recent years.

The pore connectivity of MCM-49/ZSM-5 co-crystallized zeolites were studied by Liu et al. [46] Fig. 4 shows the HP ^{129}Xe NMR spectra between co-crystallized and mechanically mixed zeolites at 153 K and 143 K. At this temperature, the Xe exchanges quite slow in different pores of each zeolite, so the single signal of MCM-49 and ZSM-35 in the ^{129}Xe NMR may represent the characteristic structure themselves. In the spectra of co-crystallized and mechanically mixed zeolites, the signals of low-field and high-field are ascribed to Xe gas adsorbed in MCM-49 and ZSM-35 analogues, respectively. However, the signal in the high-field moving to the lower field compared to the pure ZSM-35 zeolite, because the Xe atoms exchange in the two different areas. At 143 K, the chemical shift difference ($\Delta\delta$) in mechanically mixed zeolites ($\Delta\delta = 65$) are more than that of co-crystallized zeolites ($\Delta\delta = 34$). It is a strong evidence to demonstrate xenon gas exchange much faster in the co-crystallized zeolite than that in mechanically mixed MCM-49 and ZSM-35 zeolites, further proved that the co-crystallized and mechanically mixed zeolites have different pore structures and connectivities.

Two-dimensional exchange spectroscopy (EXSY) HP ^{129}Xe NMR could provide more information which can help to easily detect pore structure, interconnectivity and distribution of adsorption sites [47,48], unlike other means of characterizations such as small angle X-ray and scanning electron microscope (SEM) which can only provide regional information.

Liu et al. [49] studied three types of zeolites with hierarchical pores by means of 2D-EXSY HP ^{129}Xe NMR. Fig. 5 displays the 2D-EXSY HP ^{129}Xe NMR of Meso-ZSM-5-50 and mechanical mixture composed of ZSM-5 and SiO_2 with different mixing times (τ_{mix}). In Fig. 5(a1), there are no cross-peaks appear during the mixing time less than 0.2 ms, which shows the xenon atoms have not been exchanged between micro- and meso-pores in Meso-ZSM-5-50. Then increasing τ_{mix} to 1 ms. Fig. 5(b1) shows the presence of cross-peaks which means that the exchange has been occurred at that time scale. For the mechanical mixture, Fig. 5(2) shows that even increasing τ_{mix} to 1 ms, there is still no exchange between ZSM-5 and SiO_2. Then increasing τ_{mix} to 5 ms, the cross-peaks just appeared and became stronger when extending mixing time to 10 ms. The time scale of xenon atoms exchange between ZSM-5 and SiO_2 will be slower than that in Meso-ZSM-5-50 just due to the interparticle diffusion. The different Xe adsorption behaviors indicate the characters of their hierarchical pores structure. And 2D HP ^{129}Xe NMR can intuitively demonstrated that micro-and meso-porous in the Meso-ZSM-5 may stay much closer and have better connectivity than that in mechanical mixtures.

Variable-temperature HP ^{129}Xe NMR is also an effective method to study connectivity. Recently, Wang et al. [6] used this method to study different MZSM-5. Xenon atoms are easily adsorbed in 10-membered ring channel of ZSM-5 as shown. The $\Delta\delta$ value is also a core data to evaluate the connectivity. $\Delta\delta_{MZSM\text{-}5\text{-}A}$ is 59 at 173 K, the same phenomenon are observed at 153 K and 163 K, which is lower than that of $\Delta\delta_{MZSM\text{-}5\text{-}B}$ (69), demonstrated MZSM-5-A has better interconnectivity between micro- and meso-pores than MZSM-5-B. More than that MZSM-5-A exhibited the longest lifetime during MTO catalysis process compared with MZSM-5-B and conventional ZSM-5 catalyst. In addition to ZSM-5, SAPO-34 is also a common industrial catalyst used in MTO reaction. Wang et al. [50] studied the pore connectivity of mesoporous SAPO-34 with HP ^{129}Xe NMR. In the sample SP34-MS, the low-field signals (δ 198 and 148) and high-field signal (δ 115) are ascribed to the Xe atoms absorbed in micro- and meso-porous in CHA structure. Compared with mechanically mixture which $\Delta\delta$ between micro-and meso-pore is 40, $\Delta\delta$ of SP34-MS is 33 which is less than that of previously mentioned one. This result can clearly illustrated SP34-MS has better interconnectivity between micro- and meso-pores than mechanically mixture.

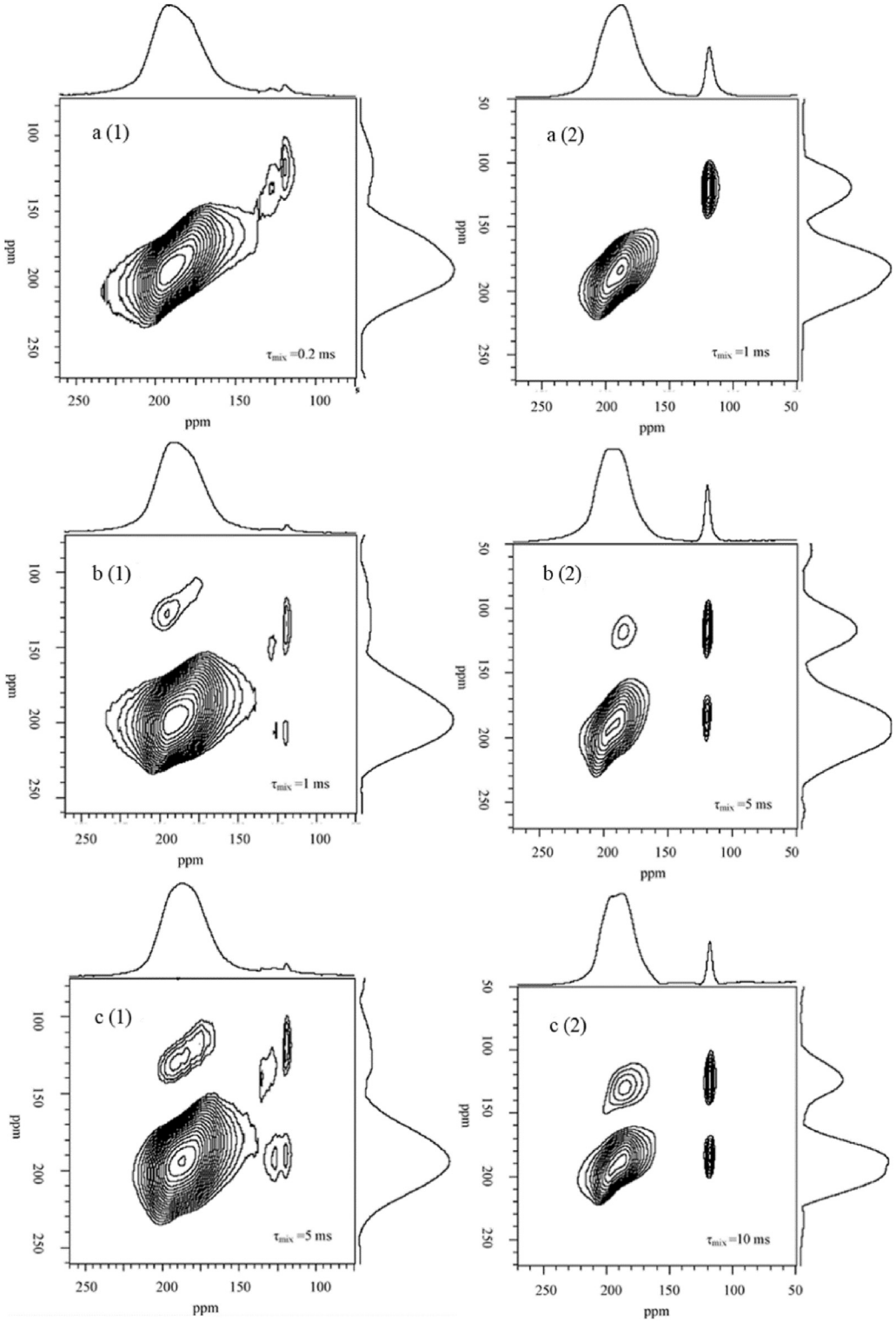

Fig. 5. HP ^{129}Xe 2D-EXSY NMR spectra of Meso-ZSM-5-50 (a(1), b(1), c(1)) and mechanically mixed conventional ZSM-5 and silica (a(2), b(2), c(2)) at 143 K with different mixing times (τ_{mix}). Adapted with permission [49]. Copyright 2008, American Chemical Society.

3.1.2. Monitoring zeolite nucleation

The crystallization of zeolite is a complicated process, which is affected by many factors, among which the most important factors are template agent, silicon source, gel composition and crystallization conditions. There are still arguments about the formation mechanism of zeolites, which can be divided into the following three viewpoints: solid phase transition, liquid phase transition and solid liquid two-phase transition mechanism.

HP ^{129}Xe NMR is a new technique which can be used to identify the pore structure changes from initial gel to crystal nucleus formation and the process of crystal growth. Valtchev and Zhang et al. [51] used variable-temperature HP ^{129}Xe NMR (see Fig. 6) to investigate the crystallization process of A-type zeolite by combing, N_2 adsorption, transmission electron microscope (TEM) and other technologies. Compared with N_2 adsorption experiments, the initial gel contains only mesopores, so the observed peak a, can be ascribed to fragments of mesopores. After half an hour of hydrothermal treatment, the peak position and strength of peak a have not changed in Fig. 6(A) and (B). In fact, this 30 min is the time which takes the reactants to reach the crystallization temperature of 90 °C. After hydrothermal treatment for an hour, great changes have taken place in the HP ^{129}Xe NMR as shown in Fig. 6(C). In addition to the peak a ascribed to the mesopores, a new peak b attribute to the birth of the first zeolite structure in the gel appears at 233 K, which provides indirect information about the change of solid structure. Lowering the temperature to 153 K and the peak b is shifted to lower field. At room temperature, the gradually disappearance of peak b is the reliable evidence of extremely low phase abundance of zeolite. Due to the strong interaction between xenon atoms and zeolite structure, the detection of the zeolite is improved a lot at low temperature. The intensity of peaks a and peak b are correlated, which means the increase of the peak b is accompanied by the decrease of the peak a as shown in Fig. 6(D). After 2 h of hydrothermal treatment, Fig. 6(E) shows that the mesoporous peak a disappeared completely in the HP ^{129}Xe NMR and only peak b is observed. It is quite surprising that there is no mesoporous can be observed at this stage. Considering the N_2 adsorption data, mesoporous components are still dominant in specimen. However, the signal of Xe atoms in micropores of zeolite can be only observed in the spectrum. The results show that nucleation process took place in the solid phase and then crystal nucleus is released into the liquid phase for crystallization. This process follows the autocatalytic mechanism. HP ^{129}Xe NMR has successfully detected the production of zeolite A with a real low concentration (<1 wt %) at the induction stage which was difficult to observe by X-ray diffraction (XRD) or TEM.

3.1.3. Location of guest species

Understanding the location of guest species is also a challenging task in zeolites. For example, in petro-chemistry, bifunctional catalysts are basically composed of metal-supported zeolites. The high acidity of zeolite is responsible for cracking and isomerization, and the metal phase is responsible for hydrogenation or dehydrogenation reactions. In order to improve the efficiency of catalytic reactions, it is a good method to introduce specific chemical species, such as cations, metal particles or oxides into the pores of zeolites [52]. So, it is very crucial to detect the definite location of guest species in zeolites for better understanding the mechanism of catalytic reaction.

HP ^{129}Xe probe can provide the distribution of guest species of entire sample compared to the TEM, which can only display local information. Zhang et al. [53] used HP ^{129}Xe probe to study the distribution of gallium atoms as the gallium concentration increasing in MCM-41 zeolite at different temperatures which is shown in Fig. 7. As the gallium concentration increased from 18.6 wt % to 65.1 wt % at 298 K, the peak intensity of xenon at δ 80 decreases with the increasing of Ga loading and the chemical displacement is almost the same as that of the main mesochannel of MCM-41. Meanwhile, a new signal at δ 100 appears in the lower field. This larger chemical shift is still in the range of mesopores. Lowering the temperature to 193 K and 233 K, the signal at low-field becomes sharper and stronger. With the increasing of Ga loading, its intensity increases gradually at the expense of the proximal signal at the higher field with increasing gallium loadings. Based on these results, the signal at higher field is ascribed to xenon gas adsorbed in the empty mesochannels of MCM-41, the lower field signal attributed to xenon gas adsorbed in the mesochannels of MCM-41 which gallium guests are located. Increasing the gallium loading up to 65.1 wt %, more and more gallium atoms are adsorbed into the mesochannels of MCM-41, and a portion of gallium remains in the interparticle voids. But there are still empty mesochannels left, which indicates gallium nanocrystals are not uniformly distributed in MCM-41 zeolite.

Li et al. [54] used HP ^{129}Xe NMR to detect the distribution of Mo species in the Mo/HBeta-Al_2O_3 catalyst at different temperatures. The spectra are shown as Fig. 8 and the signal at δ 80 is ascribed to xenon gas signal adsorbed in 12-membered ring channels of HBeta zeolite. The signal at δ 103 could be assigned to xenon gas adsorbed in the pores of Al_2O_3 the signal disappears at room temperature but emerges when reducing the temperature to 173 K. Only the signal at δ 80 appears in HBeta-Al_2O_3 material because the xenon gas is easily adsorbed in micropore rather than mesopore. With the introduction of Mo species into the HBeta-Al_2O_3 material, the xenon signal shows a small displacement moved to lower field at 173 K and 153 K which indicated that a very slight amount of Mo species is located in the pores of HBeta and the pore size of HBeta is slightly reduced. The small peak at δ 103 emerges is ascribed to the signal of empty Al_2O_3. Then this signal becomes more obvious and shifts to a lower field at 153 K for the HBeta-Al_2O_3 composite supported with Mo concentration which is 4 *wt %* or 9 *wt %*. However, there is no signal from empty Al_2O_3 indicates that adding Mo species into the composite carrier could inhibit xenon gas exchange in the HBeta and Al_2O_3. It concluded that Mo species may be located at the boundary of the HBeta and Al_2O_3. Increasing Mo loading up to 9 wt % at 153 K, two new signals appear, one is δ 131 which ascribed to xenon adsorbed in empty Al_2O_3 and the other additional peak is centered at δ 145 which ascribed to xenon adsorbed in Al_2O_3 containing Mo species, because the deposition of Mo species in Al_2O_3 pores may reduce the mean free path of xenon atoms, resulting a displacement of xenon signal moved to lower field. Therefore, the HP ^{129}Xe NMR clearly shows that Mo species is not evenly

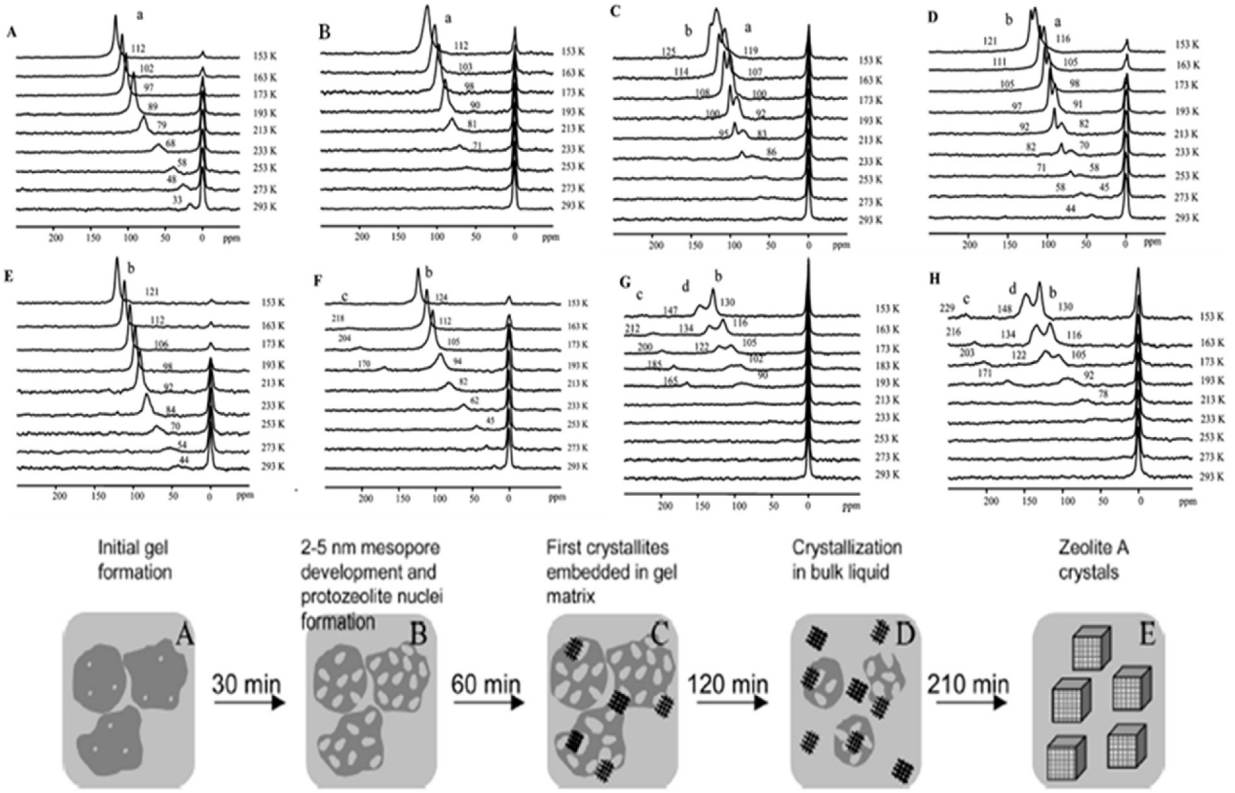

Fig. 6. Temperature-dependent HP ^{129}Xe NMR spectra of solids obtained after (A) 0, (B) 30, (C) 60, (D) 90, (E) 120, (F) 150, (G) 180, and (H) 300 min of hydrothermal treatment. And the schematic presentation of most important stages of zeolite A formation from a sodium-rich aluminosilicate system. The important stages of zeolite formation are marked with A, B, C, D, and E, respectively. Adapted with permission [51]. Copyright 2010, American Chemical Society.

distributed in HBeta and Al_2O_3 composite material. In the case of high Mo species loading, these species prefer to locate at boundary and in pores of Al_2O_3 rather than in pores of HBeta zeolites.

3.1.4. Interaction with cations

Research the setting and valence state changes of metal ions in the zeolites can be in-depth figure out the role of active center. Usually, electron spin resonance (ESR) combined with X-ray photoelectron spectroscopy (XPS) can identify the valence state of metal ions, but not provide the active site. Whereas the Xe atom is very sensitive to the change of its surrounding environment and the chemical shift difference ($\Delta\delta$) is compelling evidence to provide information about species location and influence of cations.

The faujasite (FAU) zeolite has three different kinds of structures, the super cage (S_{II}) with a twelve-membered ring (0.74 nm), the sodalite cage (S_I') with a six-membered ring (0.23 nm) and the six-prism cage (S_I) with a double-six-membered ring (0.23 nm), the cations can distribute in all three kinds of cages. Xu et al. [55] used HP ^{129}Xe NMR to study the effects in FAU zeolites with different metal cations. There are two kinds of signals in the spectra from which the δ 0 is attributed to the signal from the gas phase and the other attributes to the xenon adsorption of the super cage. The signal of 95Ag5NaX (δ −17) zeolite transferred to high field obviously at 100 °C revealed the electric field gradient generated by Ag^+ has a strong interaction to Xe nucleus and increasing shielding effects of the xenon electron cloud. Grosses [56] suggests the reason for shielding is a $4d_\pi$ - $5d_\pi$ back-donation from 4d-orbit of Ag to 5d-orbit of Xe. However, the signal of 20Ag80NaY has a little change compared with NaY, showed that the content of Ag^+ in the cage is rather low. More Ag^+ transfer to the cages with the increase of Ag^+ exchanged lead to the chemical displacement of ^{129}Xe moved to the high field. Therefore the change of chemical shift is a sensor signal to infer the setting of Ag^+. It can be observed that there is a competitive relationship between the interaction of Ag^+-Xe, and Xe—Xe. At high temperature, the chemical displacement of ^{129}Xe mainly depends on the interaction of Ag^+ -Xe, and low temperature depend on Xe—Xe. In this work, Xu also detected the other cations such as Cu^+, Cu^{2+} and Cs^+. Cu^+ shows the same results due to it similar nd^{10} electronic structure to Ag^+. In Cu^{2+} condition, the spectra will be broadened and the ^{129}Xe signal in the super cage will disappear due to its partial paramagnetism. On the other hand, Cs^+ can adsorb Xe atoms in super cage just because it has the familiar electronic structure with Xe atom, as a result, the chemical shift of ^{129}Xe moved to down-field.

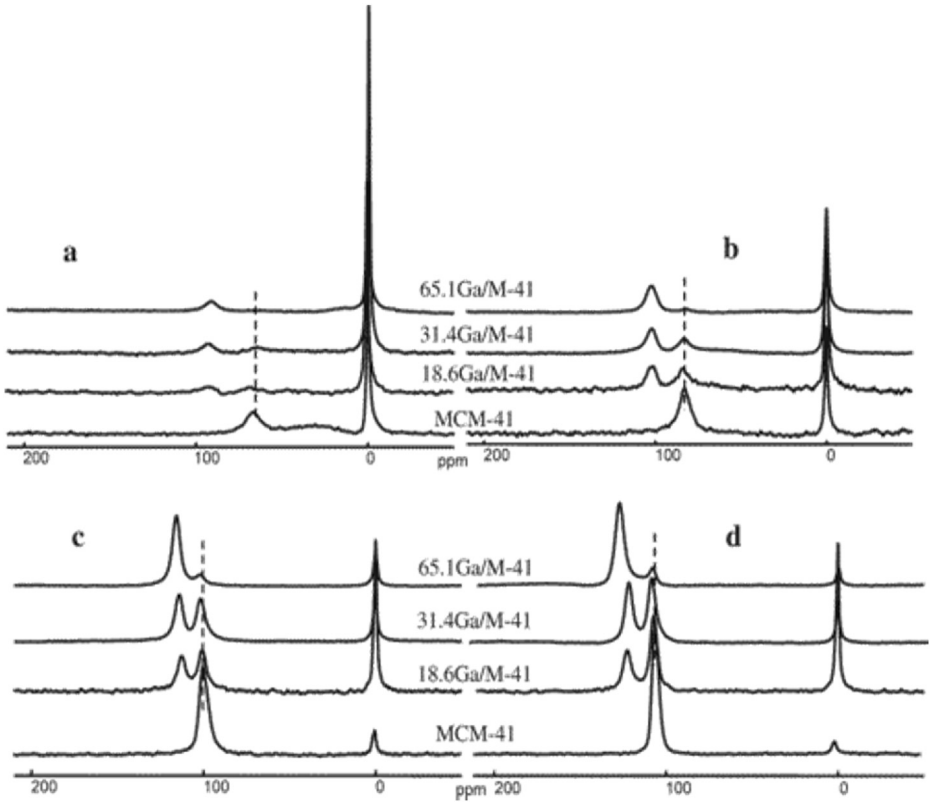

Fig. 7. HP ^{129}Xe NMR of Ga/MCM-41 mesocomposites at (a) 353 K, (b) 298 K, (c) 233 K, and (d) 193 K. Adapted with permission [53]. Copyright 2005, American Chemical Society.

3.2. Other porous materials

In recent 10 years, MOFs have been considered to be one of the most exciting developments in porous materials [57]. Two- or three-dimensional networks with many novel topologies are formed by self-assembly of metal cations and organic linkers. Most of the networks exhibited micro- or mesopores. Their adjustable apertures (0.5—3 nm), high thermal stabilities, permanent porosities, flexible frameworks and ultra-high specific surface areas, make these materials could be wildly used in many fields such as gas storage, ion-exchange, heterogeneous catalysis, sensing, separation, molecular recognition, and drug delivery [58].

MIL-53, a kind of MOF material represents flexible topologies, exists two different structures which can transfer to each other under certain conditions. One is large-pore (lp) which is an almost quadrate shape and the other is narrow-pore (np) which varied from a rhombus shape. Springuel-Huet [59] used thermal-polarized and laser-polarized ^{129}Xe NMR to study the phase transition between lp and np as shown in Fig. 9. The narrow line A at high-field is corresponding to the lp form of MIL-53 and with xenon pressure increase, a broad anisotropic line B at low-field is ascribed to np form. Reducing the temperature from 222 K to 218 K, the lp signal A gradually decreases until disappears while the np signal B appears and gradually strengthens indicating the transformation from lp to np has been occurred and completed in MIL-53. So the HP ^{129}Xe NMR is an efficient and sensitive method to observe the structural transformation of MIL-53 from lp form to np form.

As a branch of MOFs, zeolitic imidazolate frameworks (ZIFs) have wide application prospects in many fields due to their versatility in transition metal centers and custom organic connectors. ZIF-8 has a sodalite topology composed of cavities with diameter of 1.16 nm and the cavities are connected by 8 windows with diameter of 0.34 nm. Even the diameter of xenon atom is larger than that of aperture, xenon atom can also be adsorbed in ZIF-8 maybe due to the flexibility of ZIF-8 structure. In 2013, Springuel-Huet [60] use the variable-temperature HP ^{129}Xe NMR to confirm the flexibility of the ZIF-8. The spectra at low temperature showing the chemical shifts of xenon atoms suddenly increasing ($\Delta\delta > 100$) in a few degrees from 170 K to 163 K, is the direct experimental evidence for structural flexibility of ZIF-8. From 153 K to 173 K, the chemical displacement of ^{129}Xe atom increases greatly, indicating that the organic connecter can be redirected. This structural change is confirmed by an increase in the xenon load of about 8 atoms per chamber at low temperatures. Rearrangement of adsorbed phase may occur at low temperature leading to a sharp increase in chemical displacements.

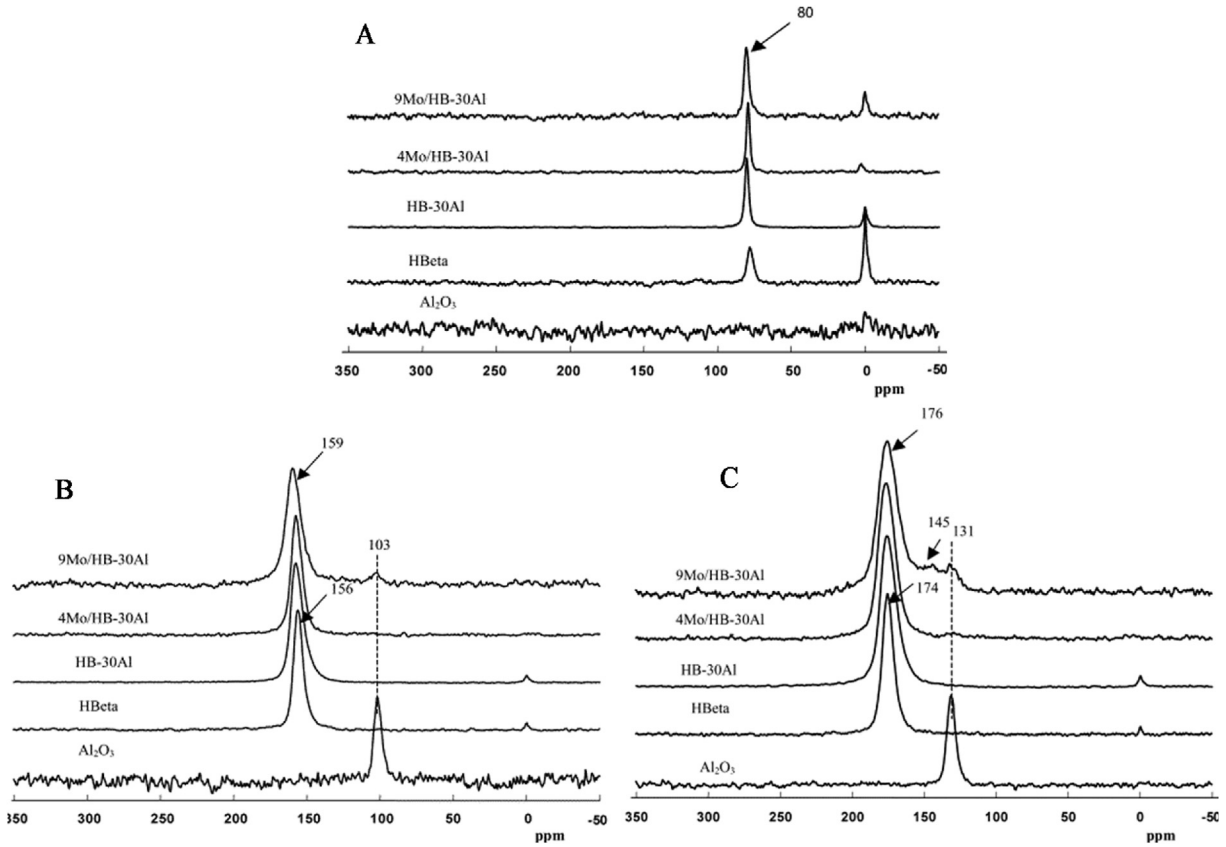

Fig. 8. Variable-temperature HP ^{129}Xe NMR spectra of HBeta zeolites, alumina, and Mo/HB-nAl catalysts acquired at (a) 293 K, (b) 173 K, (c) 153 K. Adapted with permission [54]. Copyright 2007, Elsevier.

Demarquay and Fraissard [61] established a model to calculate the mean free path in the pores of zeolites from the chemical shift of ^{129}Xe, which was successfully applied in many fields such as pillared clays and mesoporous silica materials. However, the ^{129}Xe chemical displacement experimental database of MOFs is quite limited, and only for a few examples such as IRMOFs [62], ZIF-8 [60], MIL-53 [59] and UiO-66 [9] have been published so far. Tobias et al. [63], obtained the microscopic image of ^{129}Xe chemical displacement of Xe atoms adsorbed in the CAU-1 derivatives and other reticular by DFT calculations. The interactions and dynamics of an isolated Xe atom are modeled by a large number of potential adsorption sites representing the network. A three-dimensional map of the location of Xe atom is established and two hypersurfaces, one for the energy and one for the chemical shift of ^{129}Xe, are distributed. These diagrams allow the experimental chemical displacement of ^{129}Xe to be modeled as the average total xenon atoms positions. HP ^{129}Xe NMR can fingerprint the porosity and side chain disturbance of CAU-1 frameworks and extend to other MOFs materials.

Metal nanoparticles stabilized by MOFs is a new research hotspot in recent years, however the localization of guest metal nanoparticles still face great challenges. Jiang et al. [12] studied the location of Pt and PtCu nanoparticles inside MIL-101 by using HP ^{129}Xe technique cooperated with high-angle annular dark-field scanning transmission electron microscopy (HAADF-STEM) and positron annihilation spectroscopy (PAS), and drew a conclusion that the nanoparticles are mostly embedded inside the MOF pores rather than surface. ^{129}Xe is a sensitive MOFs probe to characterize the pores and its low field signal comes from xenon molecules absorbed in the pores of MIL-101. The chemical shifts of ^{129}Xe gradually move the higher field along with the increasing percent of PtCu in MIL-101 which means that the void spaces of MIL-101 are smaller than before. The results further demonstrate that the metal nanoparticles are mainly encapsulated in MOF pores. This method will lay a foundation for the detection of guest species location in different host porous materials, thus greatly promoting the development of host-guest nanocomposites, especially in the field of catalysis.

Clays are also one of the common porous materials with broad applications because of their properties of exchangeable anion and adjustable pore size. Pillared structure of triethylamine-hectorite consists of inorganic pockets of two tetrahedral silicate layers condensed to a central magnesium oxide octahedral layer intercalated by tetraethylammonium cations. Sozzani [64] studied the interlayer nanoporosity of pillared hectorite with CF HP ^{129}Xe NMR spectra at variable temperature and demonstrated the open pore accessibility of the structure to gases.

In the early 1990s, a new class of mesoporous silica material which named M41S had attracted most attention of many researchers. Most studies concerned the representative member of the family which are MCM-41 [65] and SBA-15 [66],

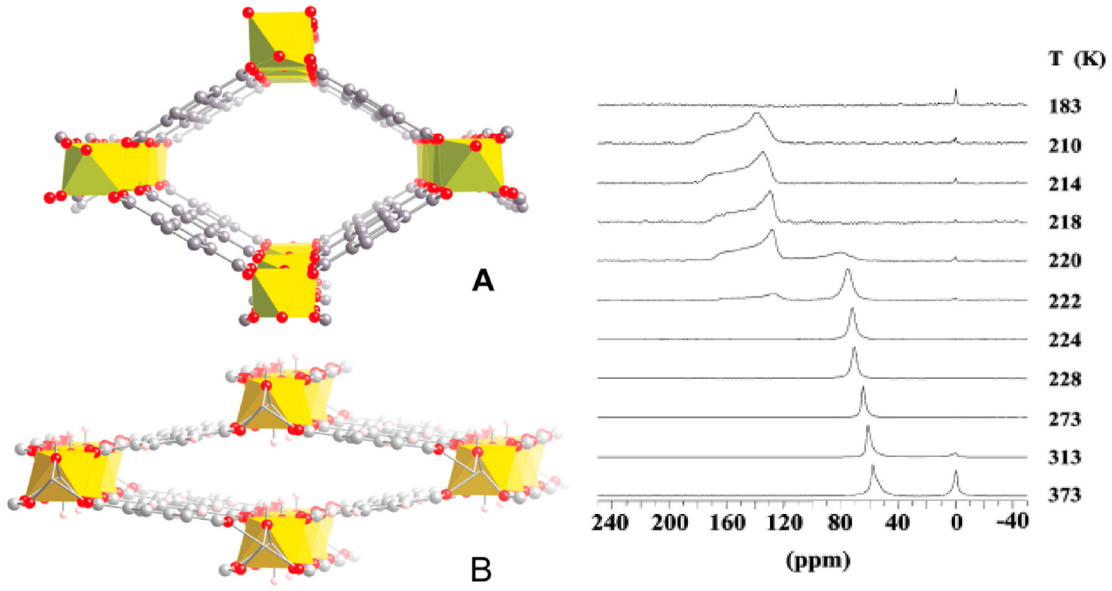

Fig. 9. Large-pore (A) and narrow-pore (B) forms of MIL-53 structure and HP ^{129}Xe NMR spectra versus temperature at $P = 1.33$ kPa. Adapted with permission [59]. Copyright 2010, American Chemical Society.

respectively. Galarneau [67] studied the dissolution and redistribution processes of silica in MCM-41 and SBA-15 materials under water treatment with variable pressure HP ^{129}Xe NMR. The differences between the local curvatures of silica in the different structures explain the difference of behavior in water with respect to silica dissolution and redeposition. Similar experiments on MCM-41 lead to a totally different dissolution and redeposition process because of its thinner walls: decrease of pore size, surface area and pore volume.

Porous carbon materials with high specific surface areas and superhydrophobicity had attracted much research interest due to their potential application in various fields including adsorption and separation of gases, energy storage and catalysis [68–70]. Saito [71] studied the xenon adsorption behavior in meso-size pores of carbon black materials using HP ^{129}Xe NMR spectroscopy. In this work, Saito first demonstrated HP ^{129}Xe NMR spectroscopy which has been shown to be successful for studying carbon black materials with Pt of the fuel cells of electric vehicles in order to decide the physisorption enthalpy.

HP ^{129}Xe NMR spectroscopy had been widely used to understand the structure of these porous materials. It has been also confirmed to be a powerful tool to obtain fast and reliable information concerning the distribution of metal particles inside the porosity or the internal structure of organically-modified porous materials. Valuable information regarding the presence of strong adsorption centers associated with modification of the chemical composition of the porous materials and the presence of an interaction between xenon and the organic phase can be obtained. Structural properties as well as heats of adsorption are obtained by combing variable pressure and temperature CF HP ^{129}Xe NMR measurements and the evolution of the ^{129}Xe NMR chemical shift [45].

4. HP ^{129}Xe NMR applied in catalytic processes

Catalysis plays a major role in the chemical industry. Approximately 85% of chemical processes use catalysts and more than 25% gross domestic product of developed countries comes from the catalytic processes [72,73]. The catalytic reaction had been considered as a black box for such a long time. So it is very crucial to explore the principle of catalytic so that the selectivity and the products can be improved a lot. Scientists have been working on the development of *in-situ* characterization techniques to reveal the process of catalytic reactions under real conditions. *In situ* NMR detecting catalytic reaction under real working conditions, which would provide extremely important signal about catalytic active sites and reaction active intermediates [74,75], is a powerful technique for the study of mechanism, kinetics and structure of catalyst at a molecular level [76]. *In situ* catalytic processes detected by HP ^{129}Xe NMR is described in detail in this section.

Anala [76] studied *in situ* combustion process of methane on NaX zeolite. Since the chemical shift of ^{129}Xe is directly related to temperature, the combustion in different areas could be observed clearly. Ripmeester [77] studied the adsorption of an organic zeolite, the result shows that *in situ* HP ^{129}Xe NMR can detect the changes from activity to inertia after adsorption of dichloromethane and the vacancy in the molecular sieve.

Xu et al. [39] studied the methanol conversion in chabazite (CHA) nanocages coupled with CF HP ^{129}Xe NMR to investigate the kinetic and dynamic processes. HP ^{129}Xe NMR spectra displays the xenon gas co-injected with methanol in CHA nanocages at 25 °C and 180 °C which corresponding to the adsorption and reaction process as shown in Fig. 10(a) and (b). At

25 °C, the peak at δ 84 can be ascribed to the adsorption of Xe in the empty CHA cages. The peaks at lower field are ascribed to xenon gas adsorbed in CHA cages. Continue to inject xenon gas together with methanol, another dynamic signal gradually occurs at low-field which may reasonable attributed to xenon gas and methanol adsorbed together in CHA cages. Increasing mixed feeding time to 15 min, the signal at lower field transferred to δ 99 and kept stable which means the dynamic equilibrium has been accomplished when xenon gas and methanol co-adsorbed in CHA cages. On the other hand, the signal at δ 84 which ascribed to xenon gas adsorbed in empty cages gradually decreased until disappeared. Fig. 10(b) shows the HP ^{129}Xe NMR spectra at 180 °C which reveals the reaction kinetics of methanol in CHA nanocages. With the ^{129}Xe gas and $^{13}CH_3OH$ continuous co-injected in CHA zeolite, the signal at δ 84 attributes to empty cage decreases, while the signal at δ 92 which ascribed to $^{13}CH_3OH$ adsorbed in CHA cage and δ 88 which related to $^{13}CH_3OH$ reaction in CHA cage increase. When the strength of empty cage drops to 0, the intensities of the remaining two signal are no longer change.

The kinetic curves of methanol adsorbed in CHA nanocages is obtained by fitting the second-order exponential decay equation as shown in Fig. 10(c). According to the kinetic equation $r = K_a\,[\mathrm{Cage}]^n_{\mathrm{empty}}$ (r represents the reaction rate and K_a represents the adsorption constants), the adsorption rate equation $r = K_a\,[\mathrm{Cage}]^{1.57}_{\mathrm{empty}}$ is obtained. The activation energy of methanol adsorption in the CHA nanocages could be estimated approximately 5.2 kJ/mol according to the Arrhenius equation as shown in Fig. 10(d) which indicates that methanol adsorption in CHA nanocage belongs to physical adsorption. Use the same method also successfully obtained the kinetic curves of methanol reaction process as shown in Fig. 10(e) and the apparent activation energy of active site in methanol reaction could be calculated approximately 57 kJ/mol as shown in Fig. 10(f). These kinetic parameters are obtained directly from the molecular level.

In order to further confirm the attribution of peak B at δ 88 and provide more information about dynamic exchange between different adsorption sites of HP ^{129}Xe, HP 2D-EXSY ^{129}Xe NMR is also involved as shown in Fig. 11. The occurrence of cross-peaks related to peak A in Fig. 11(a) indicates that the xenon gas exchange between peak A and gas phase occurs at the time scale of 30 ms. The other cross-peaks related to peak B appear in Fig. 11(c) indicate that the exchange of xenon gas between the peak B and gas phase occurs when the mixing time increasing to 80 ms. Thus, the xenon gas exchange rate between the peak A and gas phase is faster than that between peak B and gas phase. This phenomenon may be due to the desorption of products, which restricts the movement of xenon atoms between gas phase and CHA cages. So, it further confirms that the signal B could be assigned to HP ^{129}Xe gas and $^{13}CH_3OH$ co-adsorbed in reaction cage, in which $^{13}CH_3OH$ are converted to dimethyl ether (DME) and water on Brönsted acid site. HP ^{129}Xe NMR technique is able to study kinetic curves and apparent activation energy of the nanocage with the active site due to the high sensitivity of xenon atom, and this

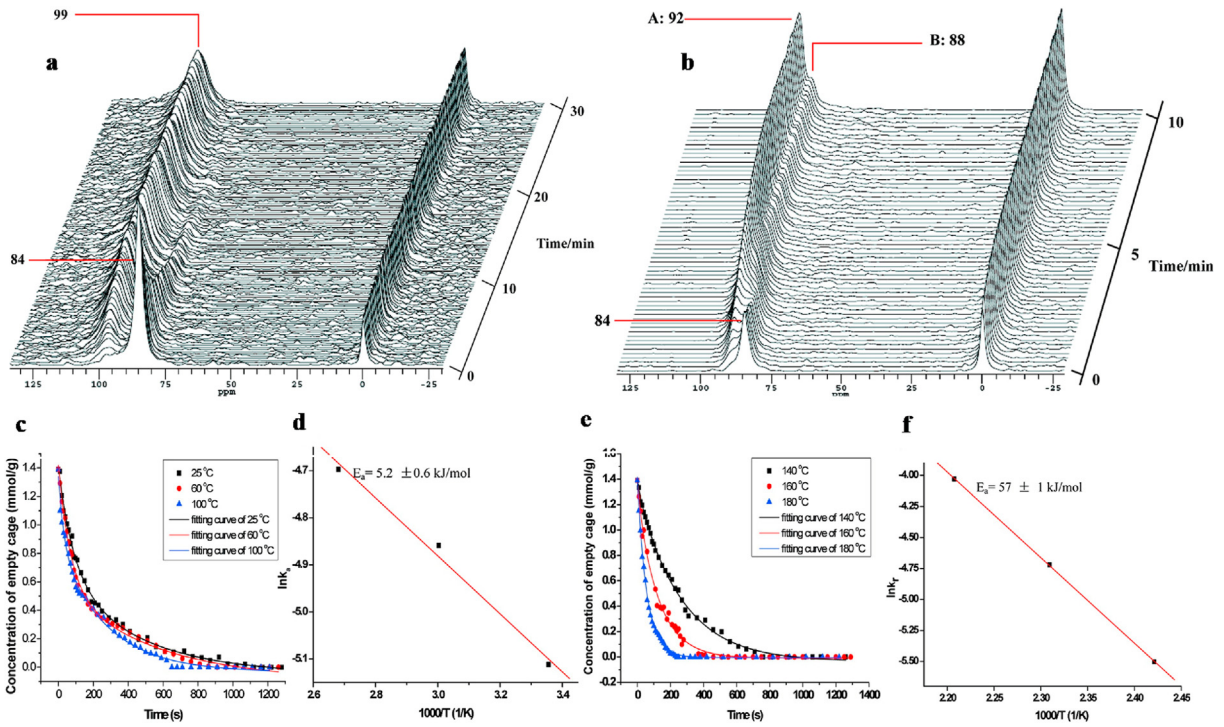

Fig. 10. *In situ* HP ^{129}Xe MAS NMR spectra recorded with a time resolution of 10 s per spectrum as a function of time during adsorption of methanol in CHA nanocages at 25 °C (a) and 180 °C (b); Kinetic curves of methanol adsorption (c) and reaction (e) in the CHA nanocages at various temperatures; (d) Arrhenius plot of rate constant K_a at different adsorption temperatures, E_a is the adsorption cativation energy; (f) Arrhenius plot of rate constants k_r at different reaction temperatures, E_a is the apparent reaction activation energy. Adapted with permission [39]. Copyright 2009, American Chemical Society.

approach can be extended to the other reactions and generally applied in the investigation of reaction kinetics in a restricted geometry under real working conditions.

Apart from adsorption and reaction kinetic, the molecular diffusion also plays a crucial role in catalytic process. Xu et al. studied [78] the methanol adsorption and desorption process in single-walled carbon nanotubes (SWNTs) compared with MCM-41 zeolite by using *in situ* CF HP ^{129}Xe NMR [Fig. 12(a) and (c)]. Methanol and HP Xenon are co-injected into the sample and then methanol gradually occupied the pore channels, resulting the adsorption signal of ^{129}Xe reduced and finally reaching a steady state. And then switch off the methanol, the adsorption signal of ^{129}Xe is gradually enhanced due to the desorption of methanol. The diffusion rate of methanol in MCM-41 and SWNT can be compared according to the change rage of ^{129}Xe signal during adsorption or desorption process. Fig. 12(b) and (d) highlight the time variation in relative peak intensities on the condition that switch on and off xenon gas which corresponding to Fig. 12 (a) and 12(c), respectively.

It was found that at −20 °C, methanol diffusion in MCM-41 nm channels is controlled by hydrogen bond interaction and van der Waals force. However, for SWNTs, it is only controlled by van der Waals force. It was also found the ^{129}Xe signal in gas phase changed significantly during adsorption and desorption in SWNTs. Further experiments proved that this is caused by the depolarization of HP ^{129}Xe caused by the strong interaction between SWNTs tube and HP ^{129}Xe. The theoretical calculation of molecular simulation shows that methanol diffusion in SWNTs nanometer channels belongs to super diffusion, and the diffusion coefficient is much higher than that of MCM-41.

5. Spin polarization transfer of Xe atom

HP ^{129}Xe can also enhance the polarizability of other nuclei (such as ^{1}H, ^{29}Si, ^{13}C) through polarization transfer, so as to improve the sensitivity of NMR [79–82]. In 1996, Pines first mixed HP ^{129}Xe which produced using optical pumping spin exchange (OPSE) method with the nuclear spin sample to be enhanced. Through the cross relaxation between them, the polarizability of HP ^{129}Xe was transferred to the nuclear spin sample which needs to be enhanced and defined as spin polarization induced nuclear Overhauser effect (SPINOE) [83]. It is a simple and practical method for improving the sensitivity of NMR signal without other conditions such as low-field thermal mixing or high-field cross-polarization. Although the polarization enhancement obtained by the SPINOE experiment of benzene for the first time is not obvious, it opens up a new application prospect for NMR.

Brunner et al. [28] first introduced the MAS method into the SPINOE experiment and observed the SPINOE phenomenon from HP ^{129}Xe to surface ^{1}H nuclei of SiO_2. Use the same device, Brunner also observed the spin polarization transferred under MAS condition from HP ^{129}Xe to^{13}C [84]. ^{129}Xe gas with the polarization of 1%–2% was injected into C_{60} and C_{70} samples at 150 K. ^{13}C signal of C_{60} was enhanced by 1.15 times at δ 144. However, in C_{70}, different positions of spin have different intensification, among which, the ^{13}C signal generated by C_2 and C_3 at δ 147 has the largest enhancement about 1.25 times. The reason for this selective enhancement may be that ^{129}Xe atom is most easily approached to this position, or that ^{129}Xe atom with hyperpolarization is adsorbed at this position and produces higher energy.

6. Conclusion and future perspective

HP ^{129}Xe NMR has been proven as a robust tool used in porous materials for probing structures, interconnectivity and functionality. It also plays an important role as a sensitive probe molecule to provide information about electronic property and position of cations in the zeolite intra-channel or intra-cavity, interactions between adsorbed species, the structural

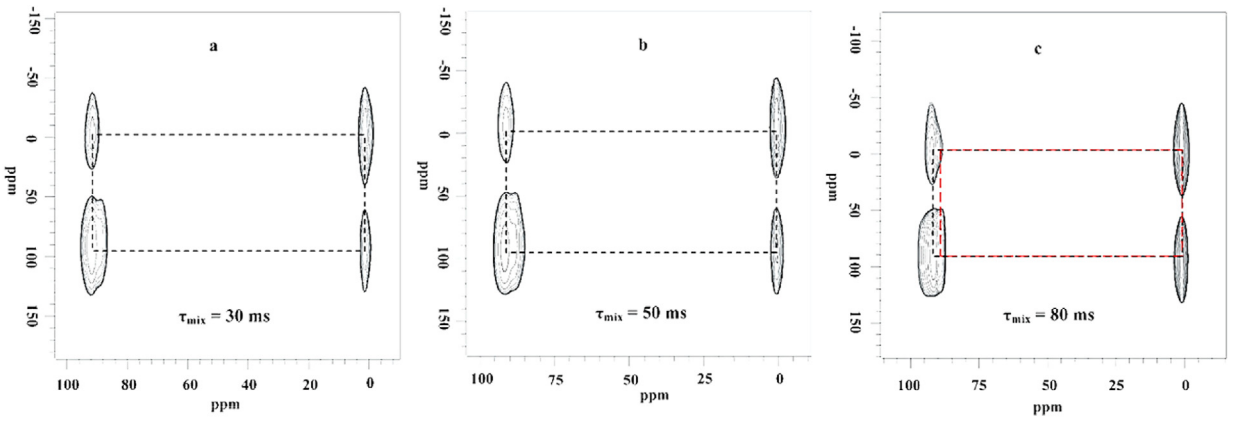

Fig. 11. *In situ* HP ^{129}Xe 2D-EXSY MAS NMR spectra recorded at 180 °C with τ_{mix} of (a) 30 ms, (b) 50 ms, and (c) 80 ms. Adapted with permission [39]. Copyright 2009, American Chemical Society..

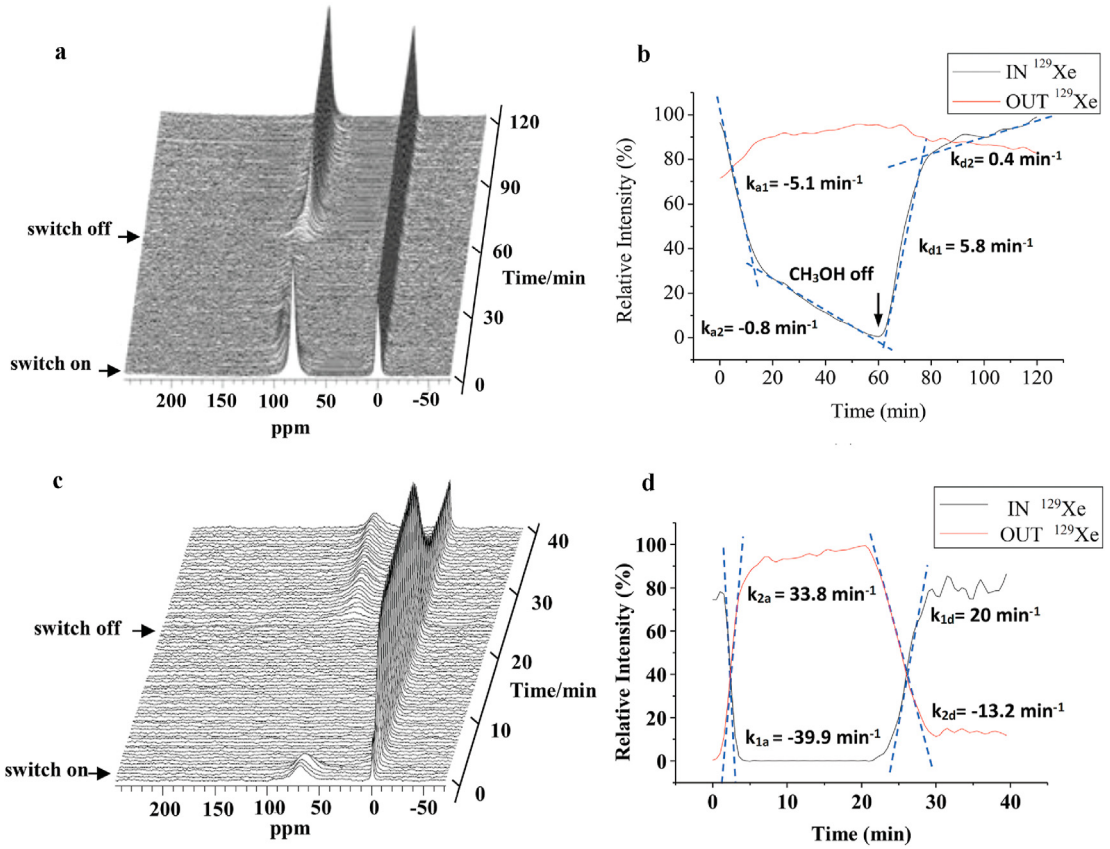

Fig. 12. *In situ* HP ^{129}Xe MAS NMR spectra recorded as a function of time, with a time resolution of 30 s per spectrum during desorption and desorption of methanol in MCM-41 (a) and SWNT (c) nanochannels at −20 °C; time variation in relative peak intensities of ^{129}Xe in MCM-41 (b) and SWNT (d) in nanochannels and in the gas phase. The solid lines represent normalized experimental data and the dashed lines are the best fits to the data of ^{129}Xe in nanochannels. Adapted with permission [79]. Copyright 2019, Royal Society of Chemistry.

flexibility of the metal-organic framework. 2D EXSY NMR spectrum is useful for obtaining the information on the pore-connectivity and dynamic exchange processes of xenon in different domains in porous materials.

In situ HP ^{129}Xe NMR corresponding with CF and MAS technique is a high efficiency method to investigate dynamics and kinetics of adsorption and reaction in the catalytic process. The advantages of HP ^{129}Xe with much higher sensitivity and shorter acquisition time allow the kinetics to be probed in a confined geometry under the continuous-flow conditions close to the real heterogeneous catalysis. As a new powerful technique, *in situ* HP ^{129}Xe NMR, in combination with other methods, is bound to give much more useful information which will help us to reveal the catalytic intermediates and catalytic processes.

Spin polarization transferred under MAS from HP ^{129}Xe to other nuclei (such as ^{1}H, ^{29}Si, ^{13}C) will provide an opportunity to investigate the host-guest interaction between Xe atom and adsorption sites of porous materials. This method has not only made achievements in the research of solid material, but also has great potential for the research of medical, biological protein and other molecules. Correspondingly, the development of this method to improve the detection sensitivity of more nuclei is also a new challenge.

Declaration of competing interest

The authors declare that they have no potential conflict of interest.

Acknowledgements

This work was supported by Natural Science Foundation of china (grant no. 22022202, 21972142, 91745109, 91545104), the LiaoNing Revitalization Talents Program (grant no. XLYC1807227). This work is dedicated to Professor Xiuwen Han on the occasion of her 80th birthday.

References

[1] J.L. Bonardet, J. Fraissard, A. GéDéON, et al., Nuclear magnetic resonance of physisorbed ^{129}Xe used as a probe to investigate porous solids, Cat Rev-Sci Eng 41 (2) (1999) 115–225.
[2] T. Pietrass, H.C. Gaede, Optically polarized Xe-129 in NMR-spectroscopy, Adv. Mater. 7 (10) (1995) 826–838.
[3] T. Ito, J. Fraissard, ^{129}Xe NMR study of xenon adsorbed on Y zeolites, J. Chem. Phys. 76 (11) (1982) 5225–5229.
[4] J.A. Ripmeester, Nuclear shielding of trapped xenon obtained by proton-enhanced, magic-angle spinning xenon129 NMR spectroscopy, J. Am. Chem. Soc. 104 (1) (1982) 289–290.
[5] L.Y. Wang, P. Tian, Y.Y. Yuan, et al., Seed-assisted synthesis of high silica ZSM-35 through interface-induced growth over MCM-49 seeds, Microporous Mesoporous Mater. 196 (2014) 89–96.
[6] Q.Y. Wang, S.T. Xu, J.R. Chen, et al., Synthesis of mesoporous ZSM-5 catalysts using different mesogenous templates and their application in methanol conversion for enhanced catalyst lifespan, RSC Adv. 4 (41) (2014) 21479–21491.
[7] L.H. Chen, S.T. Xu, X.Y. Li, et al., Multimodal Zr-Silicalite-1 zeolite nanocrystal aggregates with interconnected hierarchically micro-meso-macroporous architecture and enhanced mass transport property, J. Colloid Interface Sci. 377 (1) (2012) 368–374.
[8] H. Bunzen, F. Kolbe, A. Kalytta Mewes, et al., Achieving large volumetric gas storage capacity in metal-organic frameworks by kinetic trapping: a case study of Xenon loading in MFU-4, J. Am. Chem. Soc. 140 (32) (2018) 10191–10197.
[9] K. Trepte, J. Schaber, S. Schwalbe, et al., The origin of the measured chemical shift of (129)Xe in UiO-66 and UiO-67 revealed by DFT investigations, Phys. Chem. Chem. Phys. 19 (15) (2017) 10020–10027.
[10] Y.X. Ma, Z.J. Li, L. Wei, et al., A dynamic three-dimensional covalent organic framework, J. Am. Chem. Soc. 139 (14) (2017) 4995–4998.
[11] R. Giovine, C. Volkringer, M.A. Springuel Huet, et al., Study of xenon mobility in the two forms of MIL-53(Al) using solid-state NMR spectroscopy, J. Phys. Chem. C 121 (35) (2017) 19262–19268.
[12] Y.Z. Chen, B. Gu, T. Uchida, et al., Location determination of metal nanoparticles relative to a metal-organic framework, Nat Common 10 (1) (2019) 3462–3472.
[13] A. Comotti, S. Bracco, P. Sozzani, et al., Nanochannels of two distinct cross-sections in a porous Al-based coordination polymer, J. Am. Chem. Soc. 130 (41) (2008) 13664–13672.
[14] B.M. Goodson, Nuclear magnetic resonance of laser-polarized noble gases in molecules, materials, and organisms, J. Magn. Reson. 155 (2) (2002) 157–216.
[15] S. Xiao, H. Deng, C.H. Duan, et al., Considering low-rank, sparse and gas-inflow effects constraints for accelerated pulmonary dynamic hyperpolarized (129)Xe MRI, J. Magn. Reson. 290 (2018) 29–37.
[16] J.H. Xie, H.D. Li, H.T. Zhang, et al., Single breath-hold measurement of pulmonary gas exchange and diffusion in humans with hyperpolarized (129) Xe MR, NMR Biomed. 32 (5) (2019) 4068–4079.
[17] S.J. Yang, Y.P. Yuan, W.P. Jiang, et al., Hyperpolarized (129) Xe magnetic resonance imaging sensor for H_2S, Chem. Eur J. 23 (32) (2017) 7648–7652.
[18] B. Zhang, Q.N. Guo, Q. Luo, et al., An intracellular diamine oxidase triggered hyperpolarized (129)Xe magnetic resonance biosensor, Chem. Commun. 54 (97) (2018) 13654–13657.
[19] H.T. Zhang, J.S. Xie, S. Xiao, et al., Lung morphometry using hyperpolarized (129) Xe multi-b diffusion MRI with compressed sensing in healthy subjects and patients with COPD, Med. Phys. 45 (7) (2018) 3097–3108.
[20] A. Kastler, Quelques suggestions concernant la production optique et la détection optique d'une inégalité de population des niveaux de quantifigation spatiale des atomes. Application à l'expérience de Stern et Gerlach et à la résonance magnétique, J. Phys. Radium 11 (6) (1950) 255–265.
[21] M.A. Bouchiat, T.R. Carver, C.M. Varnum, Nuclear polarization in He-3 gas induced by optical pumping and dipolar exchange, Phys. Rev. Lett. 5 (8) (1960) 373–375.
[22] S.R. Schaefer, G.D. Cates, T.R. Chien, et al., Frequency shifts of the magnetic-resonance spectrum of mixtures of nuclear spin-polarized noble gases and vapors of spin-polarized alkali-metal atoms, Phys Rev A 39 (11) (1989) 5613–5623.
[23] D. Raftery, H. Long, T. Meersmann, et al., High-field NMR of adsorbed xenon polarized by laser pumping, Phys. Rev. Lett. 66 (5) (1991) 584–587.
[24] X.Z. Zeng, C.J. Wu, M.X. Zhao, et al., Laser-enhanced low-pressure gas NMR signal from Xe-129, Chem. Phys. Lett. 182 (6) (1991) 538–540.
[25] E. Brunner, Enhancement of surface and biological magnetic resonance using laser-polarized noble gases, Concepts Magn. Reson. 11 (5) (1999) 313–335.
[26] A.M. Oros, N.J. Shah, Hyperpolarized xenon in NMR and MRI, Phys. Med. Biol. 49 (20) (2004) 105–153.
[27] D. Raftery, E. Macnamara, G. Fisher, et al., Optical pumping and magic angle spinning: sensitivity and resolution enhancement for surface NMR obtained with laser-polarized xenon, J. Am. Chem. Soc. 119 (37) (1997) 8746–8747.
[28] E. Brunner, R. Seydoux, M. Haake, et al., Surface NMR using laser-polarized (129)Xe under magic angle spinning conditions, J. Magn. Reson. 130 (1) (1998) 145–148.
[29] J.F. Haw, In situ NMR of heterogeneous catalysis: new methods and opportunities, Top. Catal. 8 (1–2) (1999) 81–86.
[30] M. Hunger, T. Horvath, A new MAS NMR probe for in situ investigations of hydrocarbon conversion on solid catalysts under continuous-flow conditions, J. Chem. Soc., Chem. Commun. (14) (1995) 1423–1424.
[31] P. Goguen, J.F. Haw, An in situ NMR probe with reagent flow and magic angle spinning, J. Catal. 161 (2) (1996) 870–872.
[32] E. Macnamara, D. Raftery, A high-resolution solid-state NMR probe for in-situ studies of heterogeneous catalysis under flowing conditions, J. Catal. 175 (1) (1998) 135–137.
[33] P.K. Isbester, A. Zalusky, D.H. Lewis, et al., NMR probe for heterogeneous catalysis with isolated reagent flow and magic-angle spinning, Catal. Today 49 (4) (1999) 363–375.
[34] C. Keeler, J.C. Xiong, H. Lock, et al., A new in situ chemical reactor for studying heterogeneous catalysis by NMR: the grass hopper, Catal. Today 49 (4) (1999) 377–383.
[35] A. Nossov, F. Guenneau, M.-A. Springuel-Huet, et al., Continuous flow hyperpolarized 129Xe-MAS NMR studies of microporous materials, Phys. Chem. Chem. Phys. 5 (20) (2003) 4479–4483.
[36] M. Hunger, W. Wang, Formation of cyclic compounds and carbenium ions by conversion of methanol on weakly dealuminated zeolite H-ZSM-5 investigated via a novel in situ CF MAS NMR/UV-Vis technique, Chem. Commun. (5) (2004) 584–585.
[37] W. Wang, Y.J. Jiang, M. Hunger, Mechanistic investigations of the methanol-to-olefin (MTO) process on acidic zeolite catalysts by in situ solid-state NMR spectroscopy, Catal. Today 113 (1–2) (2006) 102–114.
[38] Y.J. Jiang, J. Huang, V.R.R. Marthala, et al., In situ MAS NMR-UV/Vis investigation of H-SAPO-34 catalysts partially coked in the methanol-to-olefin conversion under continuous-flow conditions and of their regeneration, Microporous Mesoporous Mater. 105 (1–2) (2007) 132–139.
[39] S.T. Xu, W.P. Zhang, X.C. Liu, et al., Enhanced in situ continuous-flow MAS NMR for reaction kinetics in the nanocages, J. Am. Chem. Soc. 131 (38) (2009) 13722–13727.
[40] J. Rouquerol, D. Avnir, C.W. Fairbridge, et al., Recommendations for the characterization of porous solids, Pure Appl. Chem. 66 (8) (1994) 1739–1758.
[41] S.J. Huang, S. Huh, P.S. Lo, et al., Hyperpolarized ^{129}Xe NMR investigation of multifunctional organic/inorganic hybrid mesoporous silica materials, Phys. Chem. Chem. Phys. 7 (16) (2005) 3080–3087.
[42] S.J. Huang, C.H. Huang, W.H. Chen, et al., Probing the alkyl ligands on silylated mesoporous MCM-41 using hyperpolarized 129Xe NMR spectroscopy, J. Phys. Chem. B 109 (2) (2005) 681–684.
[43] A. Sakthivel, S.J. Huang, W.H. Chen, et al., Replication of mesoporous aluminosilicate molecular sieves (RMMs) with zeolite framework from mesoporous carbons (CMKs), Chem. Mater. 16 (16) (2004) 3168–3175.
[44] J. Čejka, A. Corma, S.I. Zones, Zeolites and Catalysis: Synthesis, Reactions and Applications, Wiley-VCH press, Weinheim, 2010.

[45] E. Weiland, M.-A. Springuel Huet, A. Nossov, et al., ^{129}Xenon NMR: review of recent insights into porous materials, Microporous Mesoporous Mater. 225 (2016) 41–65.
[46] Y. Liu, W.P. Zhang, S.J. Xie, et al., Probing the porosity of cocrystallized MCM-49/ZSM-35 zeolites by hyperpolarized Xe-129 NMR, J. Phys. Chem. B 112 (4) (2008) 1226–1231.
[47] A. Comotti, S. Bracco, P. Valsesia, et al., 2D multinuclear NMR, hyperpolarized xenon and gas storage in organosilica nanochannels with crystalline order in the walls, J. Am. Chem. Soc. 129 (27) (2007) 8566–8576.
[48] C.Y. Cheng, C.R. Bowers, Direct observation of atoms entering and exiting L-Alanyl-L-valine nanotubes by hyperpolarized xenon-129 NMR, J. Am. Chem. Soc. 129 (45) (2007) 13997–14002.
[49] Y. Liu, W.P. Zhang, Z.C. Liu, et al., Direct observation of the mesopores in ZSM-5 zeolites with hierarchical porous structures by laser-hyperpolarized ^{129}Xe NMR, J. Phys. Chem. C 112 (39) (2008) 15375–15381.
[50] C. Wang, M. Yang, M.R. Li, et al., A reconstruction strategy to synthesize mesoporous SAPO molecular sieve single crystals with high MTO catalytic activity, Chem. Commun. 52 (38) (2016) 6463–6466.
[51] L. Itani, Y. Liu, W.P. Zhang, et al., Investigation of the physicochemical changes preceding zeolite nucleation in a sodium-rich aluminosilicate gel, J. Am. Chem. Soc. 131 (29) (2009) 10127–10139.
[52] S.B. Liu, L.J. Ma, M.W. Lin, et al., NMR investigation of the distribution of benzene in NaX and NaY zeolites: influence of cation location and adsorbate concentration, J. Chem. Phys. 96 (20) (1992) 8120–8125.
[53] W.P. Zhang, C.I. Ratcliffe, I.L. Moudrakovski, et al., Distribution of gallium nanocrystals in Ga/MCM-41 mesocomposites by continuous-flow hyperpolarized 129Xe NMR spectroscopy, Anal. Chem. 77 (10) (2005) 3379–3382.
[54] X.J. Li, W.P. Zhang, S.L. Liu, et al., The role of alumina in the supported Mo/Hbeta-Al_2O_3 catalyst for olefin metathesis: a high-resolution solid-state NMR and electron microscopy study, J. Catal. 250 (1) (2007) 55–66.
[55] S.T. Xu, W.P. Zhang, X.W. Han, et al., Hyperpolarized Xe-129 NMR spectroscopy investigation of metal cation-exchanged FAU zeolites, Chin. J. Catal. 30 (9) (2009) 945–950.
[56] R. Grosse, R. Burmeister, B. Boddenberg, et al., Xe-129 NMR of silver-exchanged X-type and Y-type-zeolites, J. Phys. Chem. 95 (6) (1991) 2443–2447.
[57] A. Sutrisno, Y.N. Huang, Solid-state NMR: a powerful tool for characterization of metal-organic frameworks, Solid State Nucl. Magn. Reson. 49–50 (2013) 1–11.
[58] A. Schneemann, V. Bon, I. Schwedler, et al., Flexible metal-organic frameworks, Chem. Soc. Rev. 43 (16) (2014) 6062–6096.
[59] M.A. Springuel Huet, A. Nossov, Z. Adem, et al., ^{129}Xe NMR study of the framework flexibility of the porous hybrid MIL-53(Al), J. Am. Chem. Soc. 132 (33) (2010) 11599–11607.
[60] M.A. Springuel Huet, A. Nossov, F. Guenneau, et al., Flexibility of ZIF-8 materials studied using ^{129}Xe NMR, Chem. Commun. 49 (67) (2013) 7403–7405.
[61] J. Demarquay, J. Fraissard, ^{129}Xe NMR of xenon adsorbed on zeolites: relationship between the chemical shift and the void space, Chem. Phys. Lett. 136 (3–4) (1987) 314–318.
[62] K.J. Ooms, R.E. Wasylishen, ^{129}Xe NMR study of xenon in iso-reticular metal-organic frameworks, Microporous Mesoporous Mater. 103 (1–3) (2007) 341–351.
[63] T.W. Kemnitzer, C.B.L. Tschense, T. Wittmann, et al., Exploring local disorder within CAU-1 frameworks using hyperpolarized (129)Xe NMR spectroscopy, Langmuir 34 (42) (2018) 12538–12548.
[64] P. Sozzani, S. Bracco, A. Comotti, et al., Nanoporosity of an organo-clay shown by hyperpolarized xenon and 2D NMR spectroscopy, Chem. Commun. (18) (2006) 1921–1923.
[65] C.T. Kresge, M.E. Leonowicz, W.J. Roth, et al., Ordered mesoporous molecular-sieves synthesized by a liquid crystal template mechanism, Nature 359 (6397) (1992) 710–712.
[66] D.Y. Zhao, Q.S. Huo, J.L. Feng, et al., Nonionic triblock and star diblock copolymer and oligomeric surfactant syntheses of highly ordered, hydrothermally stable, mesoporous silica structures, J. Am. Chem. Soc. 120 (24) (1998) 6024–6036.
[67] A. Galarneau, M. Nader, F. Guenneau, et al., Understanding the stability in water of mesoporous SBA-15 and MCM-41, J. Phys. Chem. C 111 (23) (2007) 8268–8277.
[68] A. Silvestre-Albero, S. Rico FRANCéS, F. RODRíGUEZ-Reinoso, et al., High selectivity of TiC-CDC for CO_2/N_2 separation, Carbon 59 (2013) 221–228.
[69] F. Rodriguez-Reinoso, The role of carbon materials in heterogeneous catalysis, Carbon 36 (3) (1998) 159–175.
[70] C. Galeano, C. Baldizzone, H. Bongard, et al., Carbon-based yolk-shell materials for fuel cell applications, Adv. Funct. Mater. 24 (2) (2014) 220–232.
[71] K. Saito, A. Kimura, H. Fujiwara, The study of Xe adsorption behavior in meso-size pores of carbon black materials using laser-polarized Xe-129 NMR spectroscopy, Magn. Reson. Imaging 21 (3/4) (2003) 401–403.
[72] H. Topsoe, Developments in operando studies and in situ characterization of heterogeneous catalysts, J. Catal. 216 (1/2) (2003) 155–164.
[73] K. Tamaru, In situ surface dynamics in heterogeneous catalysis[J], App Catal A-Genl 151 (1) (1997) 167–177.
[74] W.Y. Wang, H. Hu, J. Xu, et al., Hydrogenation reaction on Pd-Cu bimetallic catalysts:A parahydrogen induced polarization study, Chin. J. Magn. Reson. 35 (3) (2018) 269–279.
[75] W.Q. Liu, Y.H. Song, X.L. Wang, et al., In operando nuclear magnetic resonance spectroscopy study on photocatalytic methanol reforming, Chin. J. Magn. Reson. 36 (3) (2019) 298–308. ZHANG W P, XU S T, HAN X W, et al. In situ solid-state NMR for heterogeneous catalysis: a joint experimental and theoretical approach[J]. Chem Soc Rev, 2012, 41(1): 192-210.
[76] S. Anala, G.E. Pavlovskaya, P. Pichumani, et al., In situ NMR spectroscopy of combustion, J. Am. Chem. Soc. 125 (43) (2003) 13298–13302.
[77] A.V. Nossov, D.V. Soldatov, J.A. Ripmeester, In situ switching of sorbent functionality as monitored with hyperpolarized 129Xe NMR spectroscopy, J. Am. Chem. Soc. 123 (15) (2001) 3563–3568.
[78] S.T. Xu, X. Li, C. Sun, et al., Mapping the dynamics of methanol and xenon co-adsorption in SWNTs by in situ continuous-flow hyperpolarized (129)Xe NMR, Phys. Chem. Chem. Phys. 21 (6) (2019) 3287–3293.
[79] M. Haake, A. Pines, J.A. Reimer, et al., Surface-enhanced NMR using continuous-flow laser-polarized xenon, J. Am. Chem. Soc. 119 (48) (1997) 11711–11712.
[80] J. Smith, K. Knagge, L.J. Smith, et al., Investigating hyperpolarized Xe-129 and CPMAS for spin polarization transfer to surface nuclei: a model study, J. Magn. Reson. 159 (2) (2002) 111–125.
[81] K. Knagge, J. Prange, D. Raftery, A continuously recirculating optical pumping apparatus for high xenon polarization and surface NMR studies, Chem. Phys. Lett. 397 (1–3) (2004) 11–16.
[82] B.M. Goodson, Using injectable carriers of laser-polarized noble gases for enhancing NMR and MRI, Concepts Magn. Reson. 11 (4) (1999) 203–223.
[83] G. Navon, Y.Q. Song, T. Room, et al., Enhancement of solution NMR and MRI with laser-polarized xenon, Science 271 (5257) (1996) 1848–1851.
[84] E. Brunner, M. Haake, A. Pines, et al., Enhancement of C-13 NMR signals in solid C-60 and C-70 using laser-polarized xenon, Chem. Phys. Lett. 290 (1–3) (1998) 112–116.

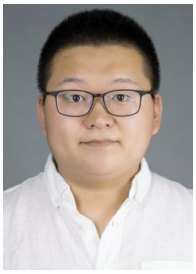

Benhan Fan received the B.S. degree in Applied Chemistry from Liaoning Normal University, Dalian in 2013. He received the M.S. degree in Physical Chemistry from Liaoning University, Shenyang in 2016. Currently he is a Ph.D. candidate at National Engineering Laboratory for Methanol to Olefins, Dalian Institute of Chemical Physics (DICP), Chinese Academy of Sciences (CAS) under the direction of Prof. Yingxu Wei and Prof. Zhongmin Liu. His research is focused on reaction mechanism catalyzed over zeolites via solid-state NMR spectroscopy.

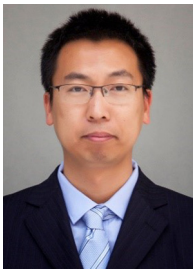

Shutao Xu received his PhD in Physical Chemistry from Dalian Institute of Chemical Physics (DICP), Chinese Academy of Sciences (CAS), in 2011. Then he joined Prof. Zhongmin Liu's team at National Engineering Laboratory for Methanol to Olefins, Dalian Institute of Chemical Physics as a research assistant. He became an associate professor in 2013 and professor in 2017. His research interests are the development of in situ NMR techniques and their applications in material science and catalysis, especially the molecular sieve synthesis and heterogeneous catalytic reaction mechanisms as revealed by in situ 1D and 2D NMR spectroscopy.

Yingxu Wei received her Ph.D. at Dalian Institute of Chemical Physics (DICP), Chinese Academy of Sciences (CAS) in 2001. She conducted her postdoctoral study at the University of Namur (Belgium) from 2003 to 2004. She has been the group leader of Catalysis and New Catalytic Reactions in the National Engineering Laboratory for Methanol to Olefins since 2009 and was promoted to professor in 2011. She has been involved in research on heterogeneous catalysis and methanol to olefin conversion.

Zhongmin Liu received his Ph.D. in Physical Chemistry from Dalian Institute of Chemical Physics (DICP), Chinese Academy of Sciences (CAS) in 1990. He has been the director of DICP since 2017. As a leading scientist, he accomplished the industrial demonstration test of DMTO technology in 2006, based on which the world's first commercial MTO unit was built up. He was elected academician of the Chinese Academy of Engineering in 2015.